

## NCEP NOTES

### Improving NCEP HWRF Simulations of Surface Wind and Inflow Angle in the Eyewall Area

WEIGUO WANG

*NOAA/National Centers for Environmental Prediction/Environment Modeling Center/I. M. Systems Group, College Park, Maryland*

JASON A. SIPPEL

*NOAA Hurricane Research Division, Miami, Florida*

SERGIO ABARCA, LIN ZHU, BIN LIU, AND ZHAN ZHANG

*NOAA/National Centers for Environmental Prediction/Environment Modeling Center/I. M. Systems Group, College Park, Maryland*

AVICHAL MEHRA AND VIJAY TALLAPRAGADA

*NOAA/National Centers for Environmental Prediction/Environment Modeling Center, College Park, Maryland*

(Manuscript received 1 October 2017, in final form 15 February 2018)

#### ABSTRACT

This note describes a modification of the boundary layer parameterization scheme in the Hurricane Weather Research and Forecasting (HWRF) Model, which improves the simulations of low-level wind and surface inflow angle in the eyewall area and has been implemented in the HWRF system and used in the operational system since 2016. The modification is on an observation-based adjustment of eddy diffusivity previously implemented in the model. It is needed because the previous adjustment resulted in a discontinuity in the vertical distribution of eddy diffusivity near the surface-layer top, which increases the friction within the surface layer and compromises the surface-layer constant-flux assumption. The discontinuity affects the simulation of storm intensity and intensification, one of the main metrics of model performance, particularly in strong tropical cyclones. This issue is addressed by introducing a height-dependent adjustment so that the vertical profile of eddy diffusivity is continuous throughout the boundary layer. It is shown that the implementation of the modification results in low-level winds and surface inflow angles in the storm's eyewall region closer to observations.

#### 1. Introduction

To adjust the initial vortex structure of a tropical cyclone (TC) in numerical models, limited observations such as flight-level and surface winds in the TC eyewall area are usually interpolated or extrapolated to other levels based on first-guess meteorological fields obtained from model output of previous hours. Therefore, it is important to accurately simulate the vertical profiles of wind in the inner-core area.

Vertical diffusion in the planetary boundary layer (PBL) is one of the most important processes governing

the vertical distribution of wind in the lower levels of the atmosphere. This process, however, cannot be fully resolved yet and in practice is parameterized because of limited model resolution. Studies have reported that the representation of vertical diffusion may have significant impacts on simulations of TC track, intensity, and structure (Braun and Tao 2000; Kepert 2012; Li and Pu 2008; Nolan et al. 2009; Smith and Thomsen 2010). While the bulk, overall structure of a TC can be simulated using most existing PBL parameterization schemes, quantitative details of the simulated fields can be significantly different using different parameterizations. For example, Smith and Thomsen (2010) compared the simulated low-level wind profiles in the eyewall area using six PBL

---

*Corresponding author:* Weiguo Wang, weigu.wang@noaa.gov

DOI: 10.1175/WAF-D-17-0115.1

© 2018 American Meteorological Society. For information regarding reuse of this content and general copyright information, consult the [AMS Copyright Policy](https://www.ametsoc.org/PUBSReuseLicenses) ([www.ametsoc.org/PUBSReuseLicenses](https://www.ametsoc.org/PUBSReuseLicenses)).

schemes and found significant discrepancies. In addition, none of the simulations gave a satisfactory profile when compared with composited observations. In another report, [Kepert \(2012\)](#) discussed the advantages and disadvantages of a variety of PBL schemes for TC simulations and concluded that caution needs to be taken when results are interpreted and that there might be need for tuning to compare with observations.

The PBL scheme in the NCEP operational Hurricane Weather Research and Forecast (HWRF) Model has its roots in the PBL scheme of the NCEP Global Forecast System (GFS). The scheme uses a parametric profile of eddy diffusivity  $K$  matching the value in the surface layer to represent local diffusion in the PBL, often referred to as the  $K$ -profile method. Surface fluxes are estimated based on the similarity theory under the constant-flux assumption (i.e., vertical flux is assumed to be independent of height in the surface layer). Due to its simplicity, stability, and low computational cost, this type of PBL scheme is being used in operational models and also has been widely employed for TC simulations by the research community ([Kepert 2012](#)). However, like many other PBL schemes, the GFS PBL scheme was originally developed to characterize the PBL over land, and it is not necessarily suitable for the tropical cyclone environment where very strong wind conditions prevail. It has been shown that in strong wind environments, the GFS PBL scheme tends to simulate deep and strong mixing, usually resulting in simulated storms of large size and weak intensity (e.g., [Gopalakrishnan et al. 2013](#); [Kepert 2012](#); [Smith and Thomsen 2010](#)). The implementation of the GFS PBL scheme in HWRF includes a method for estimating the PBL height and an eddy-diffusivity adjustment ([Tallapragada et al. 2015](#)), which are intended to make the PBL scheme suitable for TC simulations.

In this work, a further modification of the HWRF  $K$ -profile parameterization is described, and it is shown to more accurately represent low-level wind profiles and inflow angles in the eyewall area when compared with observations. This modification has been used in the operational system since 2016. In this note, HWRF simulations using an idealized configuration are first analyzed to illustrate the impact of the modification on TC simulations. Then, simulations from the operational system are analyzed to assess the impact on the overall performance. [Section 2](#) reviews the  $K$ -profile parameterization used in HWRF, followed by the modification. [Section 3](#) presents the idealized configuration of HWRF. [Section 4](#) compares low-level wind profiles and surface inflow angles in the eyewall area from different simulations using different eddy-diffusivity profiles with composite observations documented in the literature ([Franklin et al. 2003](#); [Vickery et al. 2009](#); [Zhang and Uhlhorn 2012](#)). The

intensity and track of real storms simulated by the operational HWRF system with and without the modification are also compared with observations, showing that the modification reduces the intensity error and bias. [Section 5](#) presents a summary and our conclusions.

## 2. $K$ profile in the operational HWRF Model

### a. Brief review

In the GFS and HWRF models, a subgrid vertical turbulent flux is represented using an eddy-diffusivity approach, with a nonlocal flux being added under vertically unstable conditions. A mass-flux approach, replacing the countergradient approach, was implemented in the operational GFS PBL scheme in 2015 to represent the nonlocal flux. The current operational HWRF system has used the upgraded GFS PBL scheme with modifications since 2016. The PBL parameterization in HWRF differs from that of the GFS in the estimations of PBL height and eddy diffusivity under strong wind conditions. Specific details on the parameterization are described in the HWRF Model technical documentation ([Biswas et al. 2017](#); [Tallapragada et al. 2015](#)) and references therein. Here, we only briefly review the formulation of eddy diffusivity and its modifications.

The eddy diffusivity for momentum  $K_m$  in the GFS PBL scheme ([Han et al. 2016](#); [Hong and Pan 1996](#)) is based on the work by [Troen and Mahrt \(1986\)](#). It can be written as

$$K_m = w_s \kappa z \left(1 - \frac{z}{h}\right)^p, \quad (1)$$

where  $\kappa$  is the von Kármán constant,  $z$  is the height above the surface,  $w_s$  is a velocity scale equal to  $u_* / \Phi_m$ ,  $u_*$  is the surface friction velocity,  $\Phi_m$  is a non-dimensional similarity function evaluated at the top of the surface layer  $z_s$ ,  $h$  is the PBL height (determined as the lowest level above the surface at which the bulk Richardson number is greater than a critical value), and  $p$  is a shape parameter, usually taken as a constant equal to 2, which is somewhat supported by theoretical and experimental studies ([Brost and Wyngaard 1978](#); [Troen and Mahrt 1986](#)). As  $z$  approaches zero, Eq. (1) becomes

$$K_m \approx w_s \kappa z, \quad (2)$$

which is consistent with similarity theory in which the turbulent flux is assumed to be invariable with height. The maximum value of  $K_m$  is  $4\kappa w_s h / 27$  when  $p = 2$ , and it is located at  $z_{\max} = h/3$  above the surface.

Using the GFS formulations of  $K_m$  and  $h$  in TC simulations usually results in a storm that is too diffusive with large size and weak intensity compared with other

schemes (Braun and Tao 2000; Kepert 2012; Nolan et al. 2009; Smith and Thomsen 2010). This is mainly due to  $K_m$  being too large. To address this issue, two efforts have been made to improve the performance of the scheme (Tallapragada et al. 2015).

One improvement is the estimation of  $h$  under strong wind conditions. Note that in Eq. (1),  $K_m$  is a function of  $h$ , and its maximum value is proportional to  $h$ . In HWRF,  $h$  is determined using the same bulk Richardson method as in the GFS PBL scheme except that the critical Richardson number is a function of surface wind speed or surface Rossby number (Vickers and Mahrt 2004) rather than a constant. This modification was introduced into the HWRF Model in 2013, and it lowers the simulated hurricane PBL height to values closer to the observations (Zhang et al. 2015), which led to improved simulations of hurricane intensity and size (Tallapragada et al. 2016). However, it has been suggested that modifying only the calculation of PBL height is insufficient to decrease PBL mixing in the TC environment. Kepert (2012) simulated an idealized TC using the GFS PBL scheme with a prescribed PBL height that is the same as that in other PBL schemes and found that the scheme still exhibited much larger mixing than the others considered.

The other improvement of the GFS PBL formulation made in HWRF is an adjustment of the magnitude of  $K_m$ . Gopalakrishnan et al. (2013) discovered that, at 500 m above the surface, the magnitude of  $K_m$  from the GFS PBL scheme is approximately 4 times as large as that derived from flight-level observations of a few hurricanes (Zhang et al. 2011). Therefore, they introduced a constant factor  $\alpha$  to lower the value of  $K_m$ :

$$K_{m1} = w_s k z \alpha \left(1 - \frac{z}{h}\right)^p, \quad (3)$$

where  $K_{m1}$  is the adjusted  $K_m$ . This adjustment results in significant size reductions and intensity increases in TC simulations (Gopalakrishnan et al. 2013; Zhang and Marks 2015). Zhang et al. (2015) showed that the adjustment improves the HWRF track and intensity forecasts, storm size, surface inflow angle, and near-surface wind profile.

Recently, the adjustment factor  $\alpha$  has been reformulated in HWRF to modify  $K_m$  only in regions of large wind speed, as described by Bu and Fovell (2015). In the reformulation, the adjustment factor  $\alpha$  is expressed as a function of wind speed. This new formulation caps the  $K_m$  value ( $\text{m}^2 \text{s}^{-1}$ ) at 500 m above the surface by the value of  $\text{WS}_{500}/0.6$ , where  $\text{WS}_{500}$  is the wind speed ( $\text{m s}^{-1}$ ) at the height. It is empirically based on a relation between  $K_m$  and wind speed derived from flight-level

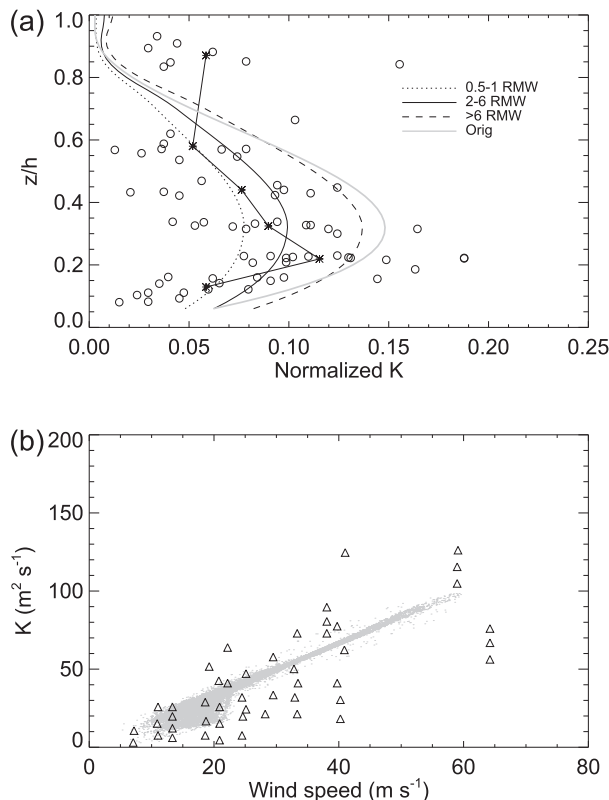


FIG. 1. (a) Vertical profiles of  $K_m$  normalized by  $\kappa w_s h$  at different locations. The RMW is about 25 km. Circles denote observation-derived results (Zhang and Drennan 2012). (b) Comparisons of  $K_m$  varying with wind speed at 500 m above the surface. Triangles stand for observation-derived results (Zhang et al. 2011) at the same level. Small gray dots show eddy diffusivity after adjustment.

observations (Zhang et al. 2011). The  $\alpha$  value calculated at 500 m is applied to all levels within the PBL. The  $K_m$  adjustment applies mostly to strong wind conditions, such as in the eyewall area.

Figure 1a shows the normalized vertical profiles of the adjusted  $K_m$  at different distances from the center of a simulated storm, along with those derived from aircraft observations (Zhang and Drennan 2012) for comparison. Note that most of the observations were located 40–220 km from the storm center and outside of the radius of maximum wind (RMW). The observation-derived  $K_m$  values are normalized using a velocity scale of  $1.3 \text{ m s}^{-1}$  and PBL height of 850 m estimated from the information provided by Zhang and Drennan (2012). Compared with its original profile,  $K_m$  is adjusted more in the area closer to the eyewall area, where the wind is stronger. Outside the eyewall area, the adjusted  $K_m$  profile is close to the original profile. The adjusted  $K_m$  profile averaged over the area between 2 and 6 RMW (approximately between 60 and 200 km in this case), corresponding to the

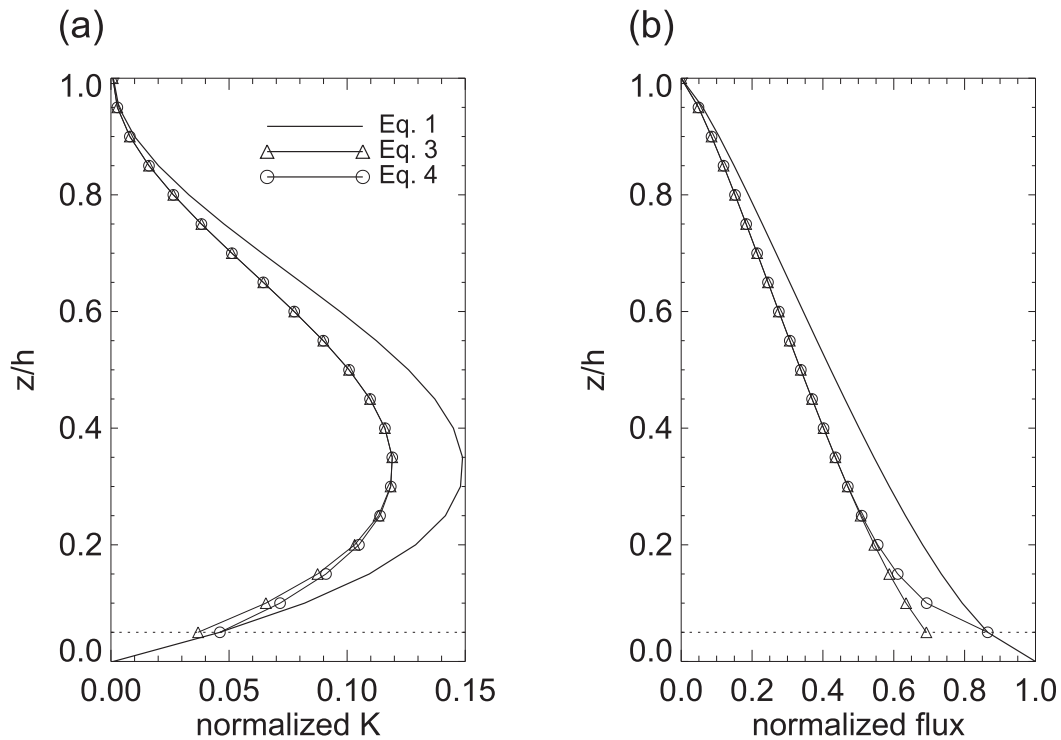


FIG. 2. (a) Vertical distributions of eddy diffusivity normalized by  $\kappa w_s h$ , from HWA1 (solid line), HWAZ (triangles), and HWAZ (circles). (b) As in (a), but for the local momentum flux normalized by the surface value, calculated using the  $K$  profiles in (a) for an assumed (given) wind profile. The dotted line shows the surface-layer top or the first level of the model above the surface.

area where observations were made, is closest to the observation-derived  $K_m$  distribution (asterisks). To further verify the modeled eddy diffusivity under strong wind conditions, flight-level observations from Hurricanes Hugo and Allen (Zhang et al. 2011) are compared with the modeled  $K_m$  at the same height (Fig. 1b), indicating that the variation of eddy diffusivity with wind speed in the model is in good agreement with that derived from observations.

b. Modification

While  $K_m$  adjustments to match the observations as the wind speed increases have resulted in better representations of vertical diffusion and model performance metrics (Bu and Fovell 2015), any adjustment that remains independent of height will yield an eddy-diffusivity profile that is not continuous at the surface-layer top (Fig. 2a).

This is because the  $K_m$  adjustment in Eq. (3) is applied only to the levels above the surface layer, but the  $K_m$  within the surface layer still follows Eq. (2). The resulting discontinuity of the magnitude of the momentum flux can be large, as illustrated in Fig. 2b, and can compromise the constant-flux assumption used within the surface layer. Furthermore, such a discontinuity of the eddy diffusivity can result in a weakening of the wind speed near the surface because the increased magnitude of flux divergence near the surface-layer top leads to a larger frictional forcing exerted on flow on the lowest (half) level of the model.

To address this issue, we provide a modification to Eq. (3) in order to give a continuous  $K_m$  profile, where the adjustment of  $K_m$  occurs gradually between the surface-layer top  $z_s$  and the level of the maximum  $K$  ( $z_{max}$ ); that is,

$$K_{m2}(z) = \begin{cases} K_m(z_s) + [K_m(z) - K_m(z_s)] \frac{\alpha K_m(z_{max}) - K_m(z_s)}{K_m(z_{max}) - K_m(z_s)}, & z_s \leq z < z_{max} \\ \alpha K_m(z), & z_{max} \leq z < h \end{cases}, \tag{4}$$

TABLE 1. Summary of experiments

Expt	Description	Remarks
HWA1	$\alpha = 1$	Original $K_m$ formulation; Eq. (1) or $\alpha = 1$ in Eq. (3)
HWAW	Wind-dependent adjustment, but height-independent $\alpha$	$K_m \leq WS_{500}/0.6$ at 500 m; Eq. (3)
HWAZ	Same as HWAW, but with height-dependent adjustment	$K_m$ is continuous at the surface-layer top, consistent with the constant flux assumption in the surface layer; Eq. (4); this is used in the current HWRP operational system

where  $K_{m2}$  is the modified  $K_m$  as shown by the solid line in Fig. 1a, and  $\alpha$  is the wind-dependent adjustment factor used in Eq. (3). Compared with Eq. (3), the adjustment factor ( $= K_{m2}/K_m$ ) is dependent not only on wind speed but also on height. Figure 2 shows that both  $K_{m2}$  and the resulting momentum flux are continuous at the surface-layer top.

### 3. HWRP Model configuration and experiments

Version 3.7a (2015) of the HWRP Model was configured for an ideal TC without ocean coupling and data assimilation and was used to test the impact of the above  $K_m$  adjustments. Three domains are used, with one parent grid and two telescopic and movable two-way nested grids. The parent domain covers approximately  $80^\circ \times 80^\circ$  with 18-km grid spacing, and the two nested grids cover  $12^\circ \times 12^\circ$  and  $7^\circ \times 7^\circ$  with 6- and 2-km horizontal grid spacings, respectively. The model uses 61 levels in the vertical (approximately 18 levels below 1000 m) with a top of 200 Pa. Time integration takes place at 30-s intervals for the parent domain and 10 and 3.3 s for nesting domains.

The GFDL surface-layer scheme (Bender et al. 2007) calculates surface fluxes and the energy budget using the observation-based momentum and enthalpy roughness lengths over water to obtain realistic surface drag coefficients. Other physics choices include the Ferrier microphysics scheme (Ferrier et al. 2002) for cloud processes, the Rapid Radiative Transfer Model (Iacono et al. 2008) for longwave and shortwave radiation, the revised simplified Arakawa–Schubert convective scheme for deep cumulus convection and a mass flux scheme for shallow cumulus convection (Han and Pan 2011) on the outer two domains, and the modified GFS PBL scheme (as described in section 2) to parameterize the subgrid-scale vertical diffusion process.

This idealized configuration assumes an  $f$  plane centered at  $15^\circ$  and a constant sea surface temperature of 302 K. The model is initialized with a mass-consistent axisymmetric cyclonic vortex (Wang 1995) superposed onto a base-state quiescent sounding. The vortex is specified with a strength of  $20 \text{ m s}^{-1}$  and a radius of

maximum wind of about 90 km. Large-scale environmental temperature and humidity fields are based on Jordan’s Caribbean sounding (Gray et al. 1975) and are assumed to be invariant with time during the entire integration. Details about the configuration of the idealized HWRP framework can be found in the 2015 HWRP scientific documentation (Tallapragada et al. 2015) and in the literature (Bao et al. 2012; Gopalakrishnan et al. 2011; Gopalakrishnan et al. 2013).

We made three simulations (Table 1) using the above-configured HWRP Model with three different  $K_m$  formulations: Eqs. (1), (3), and (4), respectively. The first simulation uses the original GFS formulation of  $K_m$ , that is, Eq. (1) or  $\alpha = 1$  in Eq. (3), which is called HWA1. The second one, denoted as HWAW, uses the wind-dependent but  $z$ -independent  $K_m$  adjustment [Eq. (3)]. The third one, denoted as HWAZ, uses the improved adjustment, which is wind and  $z$  dependent so that  $K_m$  is continuous at the surface-layer top [Eq. (4)]. The value of  $\alpha$  ranges typically from 0.6 to 1.0. It should be kept in mind that the impact of the  $K_m$  adjustment applies only to strong wind conditions and, therefore, is most apparent in the eyewall area. The model is integrated for 5 days in each simulation. The three-dimensional TC structures from the simulations are qualitatively similar to those reported in the literature (Bao et al. 2012; Gopalakrishnan et al. 2013; Gopalakrishnan et al. 2012). Therefore, we will only show basic analyses from the simulations. Our focus is on the impact of the changes in eddy diffusivity on the simulated low-level wind and surface inflow angle in the eyewall area.

### 4. Results and discussion

Figure 3 presents the time series of the maximum wind speed at 10 m above the surface from the three simulations using different  $K$  profiles. The intensity increases generally with time in spite of some fluctuations. The maximum intensity in the simulation using the wind-dependent  $K_m$  adjustment (HWAW) reaches approximately  $50 \text{ m s}^{-1}$ , while it reaches  $60 \text{ m s}^{-1}$  after the removal of discontinuity in  $K_m$  near the surface-layer top. The weaker intensity in HWAW is due to the

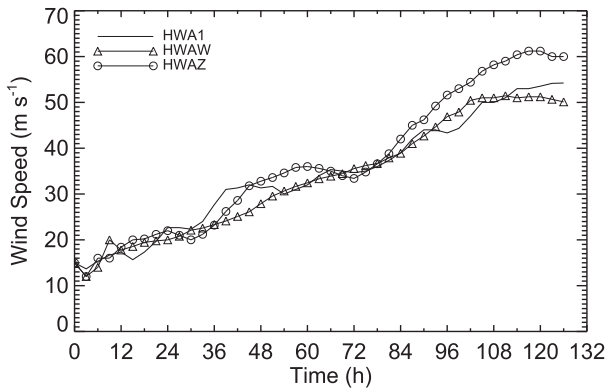


FIG. 3. The variations of vortex intensity (maximum 10-m wind speed) with time simulated by HWA1, HWAW, and HWAZ.

additional friction exerted by the  $K_m$  discontinuity, as illustrated in section 3. This is further supported by the result found when comparing the intensities from HWAW and HWA1. The intensity from HWAW is close to that from the simulation using the original  $K_m$  formulation even though the former uses an adjusted  $K_m$  that is smaller in magnitude.

Figure 4 shows a Hovmöller diagram of the contours of the azimuthally averaged tangential wind component ( $\text{m s}^{-1}$ ) at the first model level (approximately 30 m). RMWs simulated in both HWAW and HWAZ with smaller  $K_m$  magnitude in the eyewall area are smaller than that in HWA1 using the original  $K_m$  formulation. RMWs from the HWAW and HWAZ simulations are about 25 km, while it is about 40 km from the HWA1 simulation. This is a

result of the reduced  $K_m$  in the eyewall area. In addition, the reduced  $K_m$  also results in a slower broadening of the vortex (hurricane-force wind,  $33 \text{ m s}^{-1}$ ) as shown in Fig. 4. Consistent with the time series of the intensity, HWAW produces a weaker inner core than HWAZ with a slower growth rate of expansion of the hurricane-force wind due to the additional friction near the surface.

Figure 5 presents the radius–height cross section of azimuthally averaged wind components (tangential wind, radial wind, and vertical velocity;  $\text{m s}^{-1}$ ) from the three simulations at 108 h. All runs can simulate typical features of an idealized TC: maximum tangential wind below 1 km, a shallow layer of radial inflow near the surface, a deep layer of outflow in the upper troposphere, and a narrow updraft area with the existence of two maxima. Both HWAW and HWAZ simulations using the adjusted  $K_m$  profiles apparently produce a more compact vortex (smaller RMW) than HWA1 using the original  $K_m$  formulation does, with a stronger tangential wind and updraft, shallower and stronger radial inflow near the surface, and stronger outflow in the upper troposphere. With the removal of the artificial friction near the surface, HWAZ produces a narrower and stronger updraft area, and stronger tangential wind than HWAW does. For the same reason, it is suggested that the vortex of HWAW is less expanded than that of HWAZ and the depth of radial inflow layer is thinner.

To evaluate the impact of the proposed improvement on the wind profile in the hurricane eyewall area, we adopted the composite wind profiles calculated by

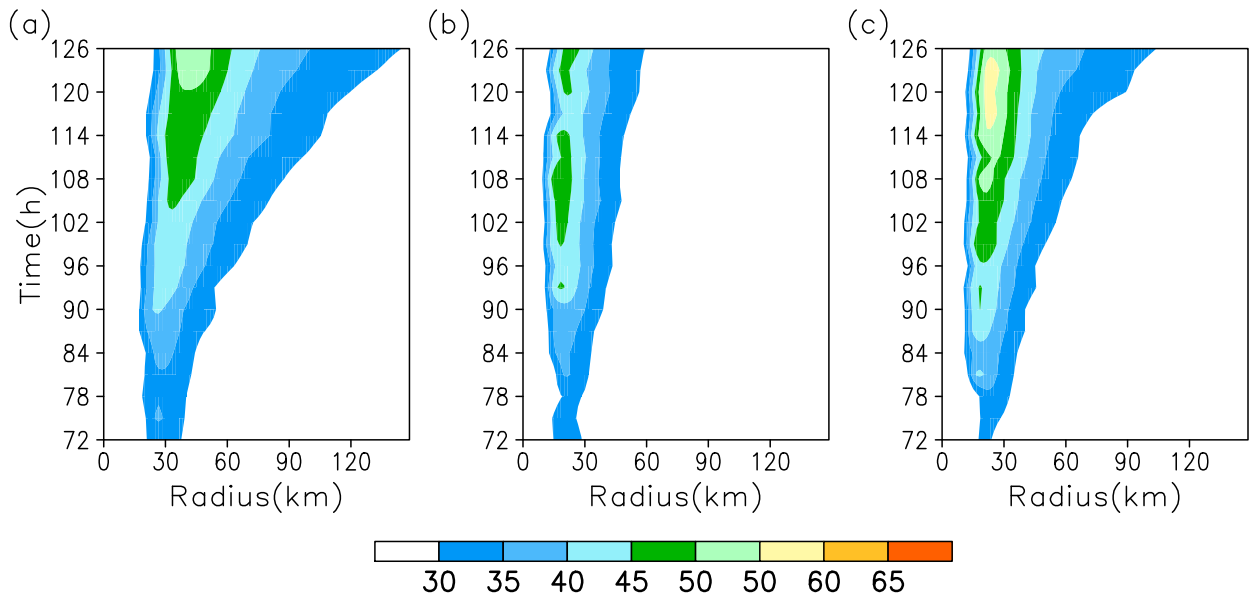


FIG. 4. Hovmöller diagrams of azimuthally averaged tangential wind speed at approximately 30 m above the surface from the (a) HWA1, (b) HWAW, and (c) HWAZ simulations.

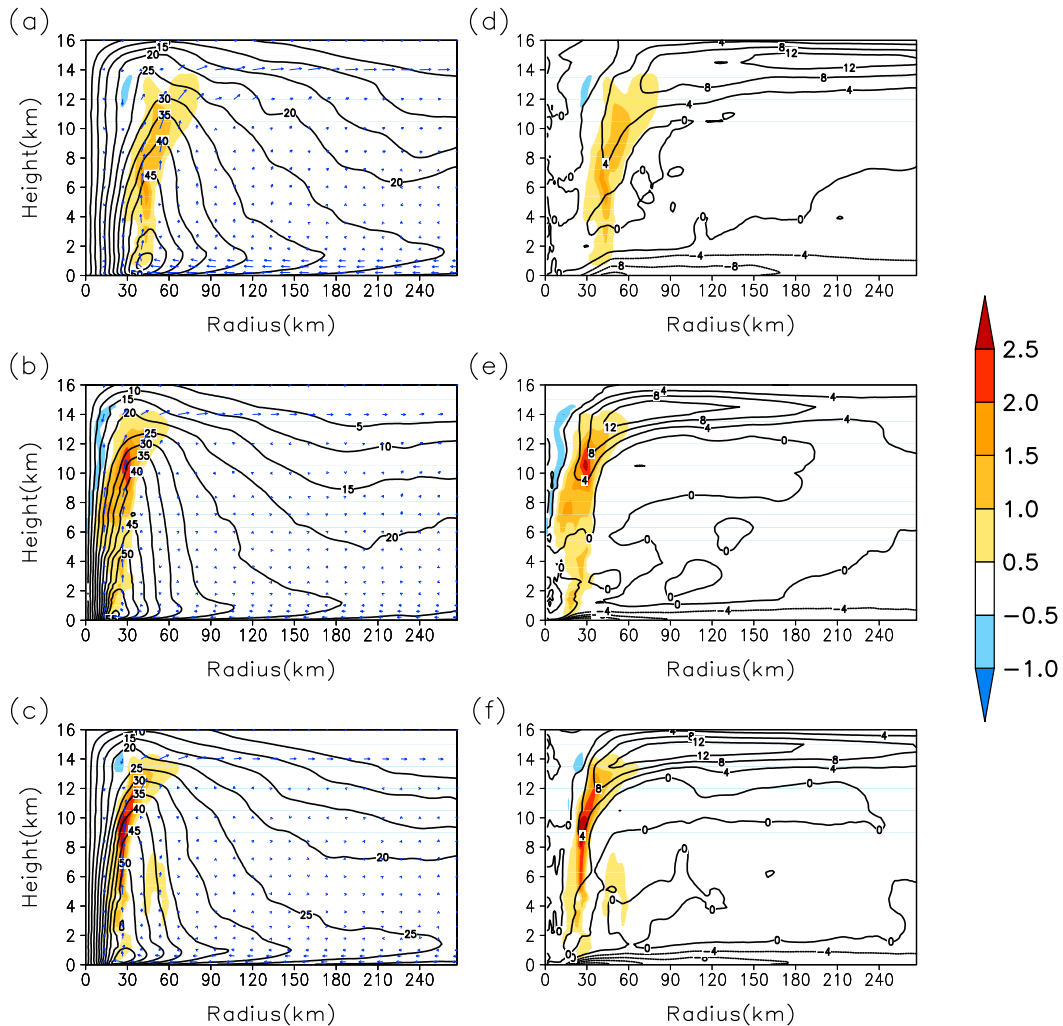


FIG. 5. Radius–height cross sections of distributions of azimuthally averaged tangential wind speed (contours), vertical velocity (shaded), and secondary circulation (vectors) at the 108th hour simulation of (a) HWA1, (b) HWAW, and (c) HWAZ. (d)–(f) As in (a)–(c), but for radial wind and vertical velocity.

Franklin et al. (2003) and Vickery et al. (2009). Franklin et al. (2003) analyzed global positioning system dropsonde soundings in the eyewall area of several hurricanes and sampled wind speed profiles based on the distance between dropsonde launch locations and the RMW at flight level (700 hPa). Vickery et al. (2009) analyzed more dropsonde data and separated the data into several categories based on RMW and mean PBL wind speed in the vortex region and the outer vortex region. Here, the wind profiles in the category where the RMW is 10–30 km and the mean PBL wind speed is 50–60  $\text{ms}^{-1}$  (Vickery et al. 2009; their Fig. 2) were selected for comparison because our simulations approximately fall into that category (in terms of RMW and mean PBL wind speed). To compare HWRF results with the composite wind profiles, we select the columns in

the TC inner cloudy area within  $0.06^\circ$  of the RMW at 700 hPa. Wind fields are sampled every 3 h after the 99th hour of each simulation when the simulated TC reaches a mature stage and the intensity changes slowly in each run (Fig. 3). The resulting profiles are compared with those in the eyewall category defined by Franklin et al. (2003) and the selected wind profiles of Vickery et al. (2009).

Following the approach used in Franklin et al. (2003), the wind speed at each level in a column is normalized by that at 700 hPa. The normalized wind speed profiles are then averaged in space and time. The resulting profiles for the three simulations are individually compared with the observed profiles in Fig. 6a. The profile from the simulation with the GFS PBL  $K_m$  formulation (HWA1) indicates that the momentum is nearly well mixed between 500 and 1500 m above the surface. The

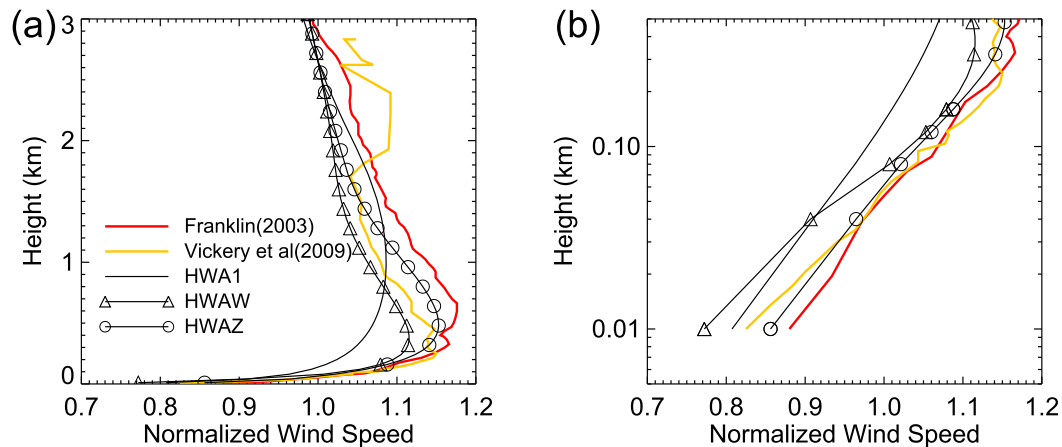


FIG. 6. (a) Vertical profiles of normalized wind speed using different  $K_m$  formulas. (b) As in (a), but for a logarithmic coordinate being used in the vertical between the surface and 0.5 km above.

maximum wind speed ratio in this simulation is about 1.09 at approximately 1000 m above the surface. This is significantly different from the average eyewall dropsonde profile shown by Franklin et al. (2003) and Vickery et al. (2009). Both observation-derived wind profiles suggest that large wind speed shear occurs in the low levels of the atmosphere, mostly within the typical PBL height. The differences below 1500 m imply that the mixing in the PBL represented by the original  $K_m$  formulation may be too strong. This is consistent with results of Gopalakrishnan et al. (2013), who showed that  $K_m$  in the original GFS PBL scheme is 4 times as large as that derived from observations under strong wind conditions.

As shown by Gopalakrishnan et al. (2013) and Bu et al. (2017), reducing the eddy diffusivity by a fraction in the HWAW simulation does increase the vertical gradient of the wind speed in the lower levels over the eyewall area (triangles in Fig. 6a). In addition, the peak value of the normalized wind speed profile is much closer to the observations than that from HWA1. Likewise, the profile from the HWAZ simulation is further improved by using the modified adjustment. The altitude of the peak wind in HWAZ (circles in Fig. 6a) better matches the observations than that in HWAW. HWAZ also gives a better simulation of wind speed in the upper PBL (e.g., 0.5–2 km) than HWAW does, though both simulations with reduced  $K_m$  generate weaker winds than the observations. This is likely due to processes such as local convection, which may not be fully represented by the surface-scaling-based  $K_m$  in the cloudy and convective environment. It is also noted that there is a large difference in wind at high levels (>2 km) between the observations and simulations. This difference might be explained by processes other than the PBL mixing, which is beyond the scope of this study. Nevertheless, the improvement

in the low-level wind profile suggests that it is very sensitive to the eddy-diffusivity parameterization.

To highlight the differences in the normalized wind speed near the surface, a logarithmic coordinate is used to replot the profiles (Fig. 6b). Both observation-derived profiles exhibit a similar vertical distribution near the surface. The normalized 10-m wind speed in HWA1 is about 0.80 (solid line in Fig. 6b), or about 9% smaller than that observed (0.88) by Franklin et al. (2003) and 2.5% smaller than that observed (0.82) by Vickery et al. (2009). This is expected since very strong PBL mixing (large  $K_m$ ) in HWA1 usually results in a weak and large storm (Fig. 5) due to strong friction forcing in the PBL. Despite its overall improvement in the vertical profiles of wind in the PBL, the HWAW simulation with less PBL mixing generates a normalized 10-m wind (0.77) (triangles in Fig. 6b) that is even lower than is seen in the observations. The weaker surface-layer winds in HWAW are likely a result of the additional flux divergence (or friction) near the surface-layer top caused by the discontinuity of the  $K_m$  profile at the surface-layer top, as illustrated in Fig. 2. After the removal of such a discontinuity, the normalized wind speed near the surface (between 10 and 100 m) for HWAZ (circles in Fig. 6b) is much improved, resembling the observed profiles. For the same reason, HWAW results in erroneously large vertical wind speed shear near the surface, but both HWA1 and HWAZ produce more realistic surface-layer speed shear.

The simulation of the surface inflow angle is affected by the vertical diffusion parameterization and, hence, by the discontinuity of the  $K_m$  profile. The mean surface inflow angle, defined as the angle of the wind vector relative to the tangential wind direction in the hurricane inner-core area, ranges typically from 20° to 25°, with large variability. Zhang and Uhlhorn (2012) analyzed

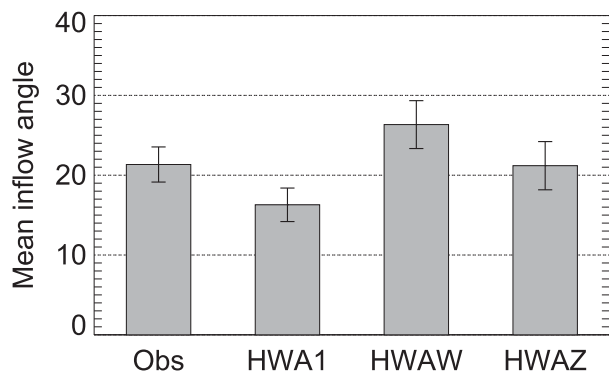


FIG. 7. Mean surface inflow angle in the eyewall area simulated from HWA1, HWA1, and HWAZ. Error bars represent the standard deviation of the mean. The mean angle derived from observations (Obs) is based on Zhang and Uhlhom (2012).

wind vector data from global positioning system dropwindsondes launched during 18 hurricanes and suggested that the mean surface inflow angle in hurricanes varies slightly with distance from the storm center, with a mean of  $22.6^\circ \pm 2.2^\circ$ . In the area near the RMW, the mean value of the inflow angle is about  $21.33^\circ$ . Figure 7 compares the mean inflow angles at 10 m above the surface and the standard deviations of the means from the three simulations. The same wind data as in the above profile analysis are used. The mean angle from HWA1 is  $16.3^\circ \pm 2.1^\circ$ , while it is  $26.3^\circ \pm 3.0^\circ$  for HWA1. Both mean values are outside of the typical range of the mean inflow angle reported in the literature. The low value of the mean inflow angle in HWA1 is probably due to weak radial winds and an overmixed PBL (Fig. 5), whereas the high value in HWA1 is due to the additional friction forcing exerted to the flow in the surface layer as a result of the discontinuity of the  $K_m$  profile. The removal of the discontinuity and the use of a smaller  $K_m$  in the PBL in HWAZ generate a better result ( $21.2^\circ \pm 3.0^\circ$ ), closer to the observed estimate ( $21.33^\circ \pm 2.2^\circ$ ).

The discontinuous  $K_m$  profile can also impact storm intensity in real simulations. We ran the operational HWRF system using the different  $K_m$  formulations (the HWAZ formulation is used in the current operational system) to simulate the entire cycles of two relatively strong storms, Hurricanes Edouard (2014) and Gonzalo (2014), initialized every 6 h. The reason to select strong storms is because the  $K_m$  adjustment is effective only for strong wind conditions. As an example to highlight the impact of the modified adjustment, Fig. 8 presents a 5-day time series of maximum surface wind speed and minimum pressure for Hurricane Edouard from the runs with the HWA1 and HWAZ  $K_m$  formulations initialized at 1800 UTC on 11 September 2014. The hurricane tracks from the two simulations are nearly the same, but the simulated

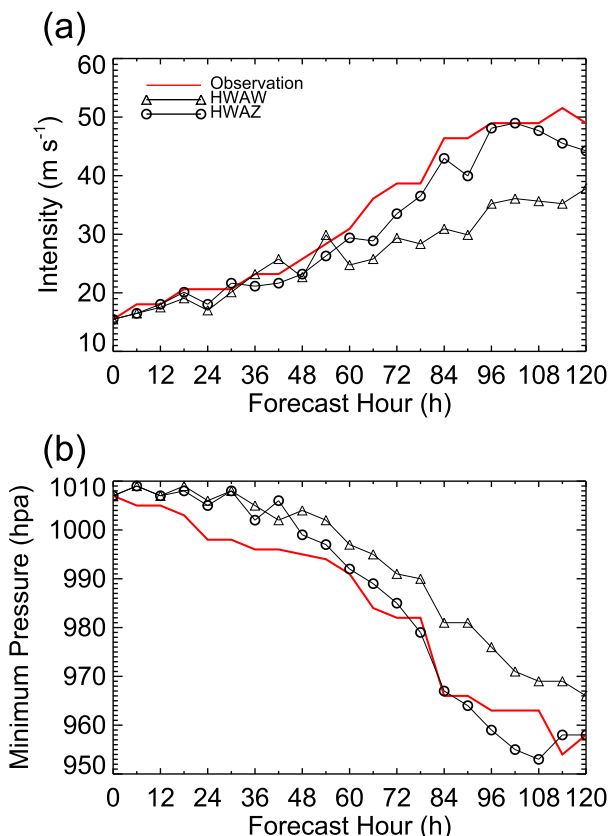


FIG. 8. Time series of (a) maximum wind speed at 10 m and (b) minimum sea level pressures simulated from the HWRF operational system before (HWA1, black solid line) and after (HWAZ, open circles) the discontinuity in the  $K_m$  profile is removed.

maximum surface wind speed (Fig. 8a) and minimum pressure (Fig. 8b) are much improved after the discontinuity of  $K_m$  is removed. The difference between the two simulations becomes more apparent after 60 h into the simulations. The larger impact in the late period of the simulation occurs because the  $K_m$  adjustment becomes effective when the wind is strong, and the impact can accumulate with time and may interact with other processes.

To assess the impact of the modification on model performance, the intensities and tracks of all simulated cycles are compared with the National Hurricane Center's (NHC) best-track data using NHC's verification package. Figure 9 shows verifications of intensity and track. The verification includes 62 verifiable cycles. The verifications of HWA1 are also shown for reference. As expected, the modified  $K_m$  adjustment improves the model performance, especially in terms of intensity. The track errors from the three runs are not much different, with HWAZ slightly reducing the track error by approximately 10% at day 5 compared with HWA1 (Fig. 9a). The intensity error in HWAZ is reduced for

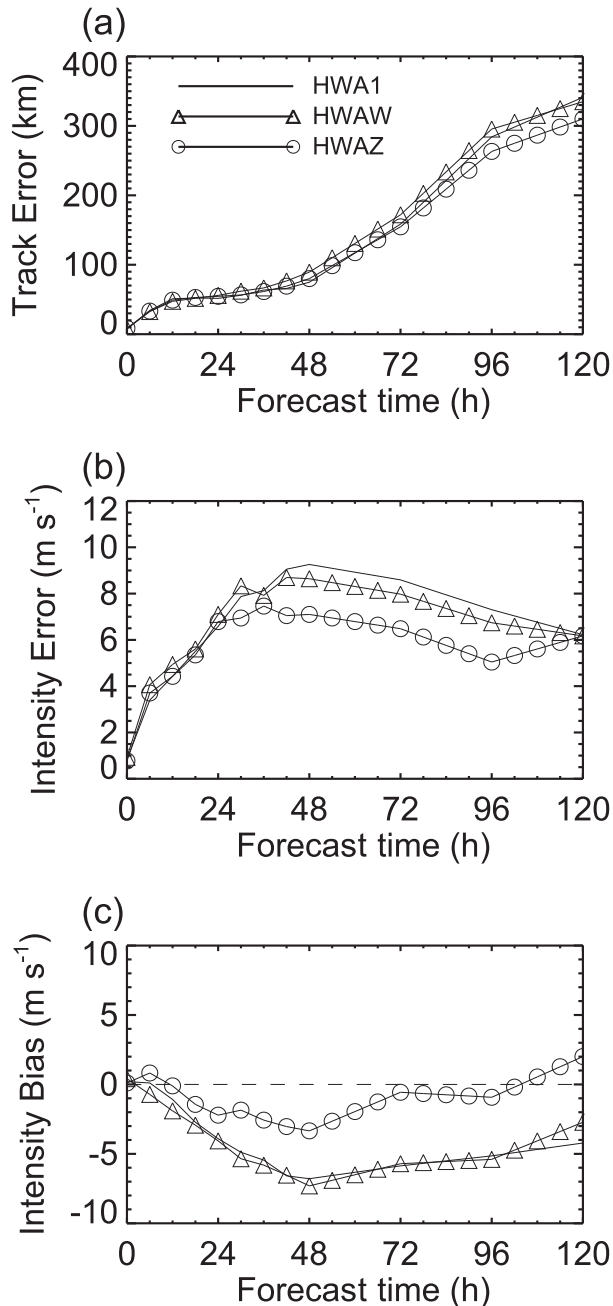


FIG. 9. (a) Mean track errors at different forecast hours from three simulations using the operational HWRf system. The verification includes 62 verifiable cycles from the simulations of Hurricanes Edouard (2014) and Gonzalo (2014). (b) Mean intensity errors (i.e., mean absolute errors). (c) Mean intensity biases (i.e., mean differences).

nearly all forecast hours compared with those in HWA1 and HWA1W (Fig. 9b), with the reduction as large as 20% between the 2- and 4-day forecasts. In general, the operational HWRf system simulated the two storms to be weaker than the observations, as indicated by negative biases for most of the forecast hours in Fig. 9c. With

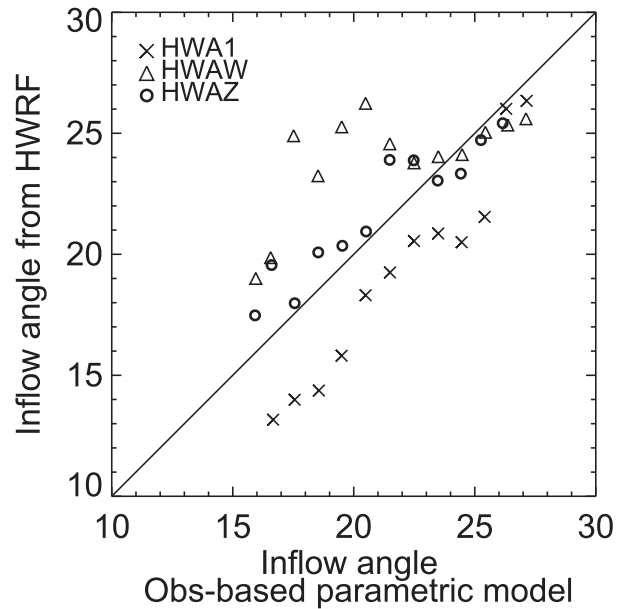


FIG. 10. Comparisons of azimuthally averaged surface inflow angles ( $^{\circ}$ ) derived from surface wind directions of HWRf output and from the observation-based parametric model (Zhang and Uhlhorn 2012). The results are averaged over an interval of  $1^{\circ}$ .

the removal of the additional friction forcing near the surface due to the discontinuity of  $K_m$ , the simulation of HWA2 is significantly less negatively biased against the observations than that of HWA1W. Compared with HWA1, HWA1W does reduce the intensity error. But the improvement of HWA1W is less significant than that of HWA2 because of the discontinuity of the  $K_m$  profile in HWA1W. To further assess the impact of the modified  $K_m$  adjustment, we calculated inflow angles at different distances from the storm center using surface wind directions over the innermost domain of each simulation. The azimuthally averaged results are compared with those calculated using the observation-based parametric model developed by Zhang and Uhlhorn (2012). The parametric model fitted the inflow angle derived from observations as a function of storm intensity and storm motion speed, as well as the distance to the storm center normalized by the RMW. Figure 10 compares the surface inflow angles derived from the HWRf wind data and from the fitted parametric model, with a 1:1 reference line plotted. The data are averaged over an interval of  $1^{\circ}$ . In general, the inflow angle of HWA2 is closest to that of the parametric model, suggesting that the surface wind structure is improved with the modification described in this note. Note that the differences in the inflow angle among the three simulations are large when the angle is small. This is because small inflow angles are likely to occur under strong local wind conditions, which is supported by data shown in Zhang and Uhlhorn (2012,

their Fig. 6). Under strong wind conditions, the  $K_m$  adjustment is activated as designed. In this case, HWA1 produces inflow angles smaller than the observation-based parametric model does, while HWAW produces significantly larger inflow angles. This is consistent with the comparison from the idealized simulations. The former can be explained by there being too much mixing in the PBL scheme in HWA1 under strong wind conditions. The latter can be explained by the additional friction forcing in HWAW that is due to the discontinuity of  $K_m$  near the surface-layer top, which makes the flow deviate more from the gradient wind. Such biases are much reduced in HWAZ. For cases with large inflow angles, the inflow angles from the three simulations are close; this is because the  $K_m$  adjustment is less likely activated under weak wind conditions, and therefore the same formation may be used in the three simulations.

## 5. Summary

This note discusses a modification to the eddy-diffusivity formulation in the PBL scheme of the HWRf Model, which has been implemented in the HWRf system. The modification improves the simulation of low-level winds and surface inflow angles in the TC eyewall area. In the past, observational studies suggested that the magnitude of eddy diffusivity  $K_m$  of the original GFS PBL scheme was much larger than that derived from measurements, especially under strong wind conditions. To address this issue, the estimation of PBL height was improved, and the magnitude of eddy diffusivity was multiplied by a height-independent fraction above the surface layer. While both changes improved the performance of the HWRf Model, it was found recently that the  $K_m$  profile was not continuous at the surface-layer top because of the height-independent adjustment fraction. This compromises the constant-flux assumption and leads to a larger flux divergence (i.e., friction forcing) near the surface-layer top, which weakens the wind speed near the surface and increases the surface inflow angle. This problem is addressed by modifying the adjusted  $K_m$  profile so that it is continuous at the surface-layer top. With the modification, the near-surface winds and inflow angle in the eyewall area are simulated closer to those derived from observations. Verifications of track and intensity from the operational HWRf system suggest that the modification can improve the overall forecast performance.

Further improvements are possible. First, our comparisons suggest that the eddy-diffusivity parameterization plays a critical role for HWRf in accurately simulating low-level winds in the TC eyewall area. Many PBL schemes available in the WRF Model including higher-order closure schemes have different vertical

distributions of eddy diffusivity in terms of their magnitude and peak location (Wang et al. 2016). Most have not yet been verified and tuned sufficiently under strong wind conditions mainly because of the difficulties involved with verification due to the lack of observations of vertical distributions of turbulent fluxes in the TC PBL. Having this in mind, we designed a few  $K_m$  profiles by keeping the same peak  $K_m$  value but changing its height. HWRf simulations with those profiles suggest that the results are highly sensitive to those changes, implying that a realistic  $K_m$  parameterization is needed for an accurate simulation of low-level wind profiles. The only way to accomplish this is to collect more observations in the TC PBL.

Also needed is an approach to better estimate PBL height, which is often used to scale PBL turbulence. Accurately determining PBL height is still challenging due partly to disagreements in how to define the TC PBL (Smith and Montgomery 2010). The usual bulk Richardson number method does not work well under strong wind conditions. While a different method with a variable critical Richardson number somewhat improves the estimation of PBL height, its performance has not yet been evaluated directly with observations. New methods are needed to determine the PBL height to better reflect the TC PBL characteristics.

Finally, the low-level wind profile in the eyewall area is also affected by other physical processes such as the surface drag and deep and shallow moist convection. Improving parameterizations of those processes should also help improve the simulations of low-level winds.

*Acknowledgments.* This work is supported by NOAA's Hurricane Forecast Improvement Project. Thanks are also due to Drs. Jongil Han and Hyun-Sook Kim for providing a thorough internal review and insightful comments.

## REFERENCES

- Bao, J. W., S. G. Gopalakrishnan, S. A. Michelson, F. D. Marks, and M. T. Montgomery, 2012: Impact of physics representations in the HWRfX on simulated hurricane structure and pressure–wind relationships. *Mon. Wea. Rev.*, **140**, 3278–3299, <https://doi.org/10.1175/MWR-D-11-00332.1>.
- Bender, M. A., I. Ginis, R. Tuleya, B. Thomas, and T. Marchok, 2007: The operational GFDL coupled hurricane–ocean prediction system and a summary of its performance. *Mon. Wea. Rev.*, **135**, 3965–3989, <https://doi.org/10.1175/2007MWR2032.1>.
- Biswas, M., and Coauthors, 2017: Hurricane Weather Research and Forecasting (HWRf) Model: 2017 scientific documentation. Developmental Testbed Center Rep., 105 pp., [https://dtcenter.org/HurrWRF/users/docs/scientific\\_documents/HWRFv3.9a\\_ScientificDoc.pdf](https://dtcenter.org/HurrWRF/users/docs/scientific_documents/HWRFv3.9a_ScientificDoc.pdf).
- Braun, S. A., and W. K. Tao, 2000: Sensitivity of high-resolution simulations of Hurricane Bob (1991) to planetary boundary layer parameterizations. *Mon. Wea. Rev.*, **128**, 3941–3961, [https://doi.org/10.1175/1520-0493\(2000\)129<3941:SOHRSO>2.0.CO;2](https://doi.org/10.1175/1520-0493(2000)129<3941:SOHRSO>2.0.CO;2).

- Brost, R. A., and J. C. Wyngaard, 1978: Model study of the stably stratified planetary boundary-layer. *J. Atmos. Sci.*, **35**, 1427–1440, [https://doi.org/10.1175/1520-0469\(1978\)035<1427:AMSOTS>2.0.CO;2](https://doi.org/10.1175/1520-0469(1978)035<1427:AMSOTS>2.0.CO;2).
- Bu, Y. P., and R. G. Fovell, 2015: Model physics influences on tropical cyclone size. *16th Conf. on Mesoscale Processes*, Boston, MA, Amer. Meteor. Soc., 17.2, <https://ams.confex.com/ams/16Meso/webprogram/Paper274629.html>.
- , —, and K. L. Corbosiero, 2017: The influences of boundary layer mixing and cloud-radiative forcing on tropical cyclone size. *J. Atmos. Sci.*, **74**, 1273–1292, <https://doi.org/10.1175/JAS-D-16-0231.1>.
- Ferrier, B. S., Y. Jin, Y. Lin, T. Black, E. Rogers, and G. DiMego, 2002: Implementation of a new grid-scale cloud and precipitation scheme in the NCEP Eta model. *19th Conf. on Weather Analysis and Forecasting/15th Conf. on Numerical Weather Prediction*, San Antonio, TX, Amer. Meteor. Soc., 10.1.
- Franklin, J. L., M. L. Black, and K. Valde, 2003: GPS dropwindsonde wind profiles in hurricanes and their operational implications. *Wea. Forecasting*, **18**, 32–44, [https://doi.org/10.1175/1520-0434\(2003\)018<0032:GDWPIH>2.0.CO;2](https://doi.org/10.1175/1520-0434(2003)018<0032:GDWPIH>2.0.CO;2).
- Gopalakrishnan, S. G., F. Marks Jr., X. J. Zhang, J. W. Bao, K. S. Yeh, and R. Atlas, 2011: The Experimental HWRf system: A study on the influence of horizontal resolution on the structure and intensity changes in tropical cyclones using an idealized framework. *Mon. Wea. Rev.*, **139**, 1762–1784, <https://doi.org/10.1175/2010MWR3535.1>.
- , S. Goldenberg, T. Quirino, X. Zhang, F. Marks Jr., K. Yeh, R. Atlas, and V. Tallapragada, 2012: Toward improving high-resolution numerical hurricane forecasting: Influence of model horizontal grid resolution, initialization, and physics. *Wea. Forecasting*, **27**, 647–666, <https://doi.org/10.1175/WAF-D-11-00055.1>.
- , F. Marks Jr., J. A. Zhang, X. Zhang, J. W. Bao, and V. Tallapragada, 2013: A study of the impacts of vertical diffusion on the structure and intensity of the tropical cyclones using the high-resolution HWRf system. *J. Atmos. Sci.*, **70**, 524–541, <https://doi.org/10.1175/JAS-D-11-0340.1>.
- Gray, W. M., E. Ruprecht, and R. Phelps, 1975: Relative humidity in tropical weather systems. *Mon. Wea. Rev.*, **103**, 685–690, [https://doi.org/10.1175/1520-0493\(1975\)103<0685:RHITWS>2.0.CO;2](https://doi.org/10.1175/1520-0493(1975)103<0685:RHITWS>2.0.CO;2).
- Han, J., and H. Pan, 2011: Revision of convection and vertical diffusion schemes in the NCEP Global Forecast System. *Wea. Forecasting*, **26**, 520–533, <https://doi.org/10.1175/WAF-D-10-05038.1>.
- , M. Witek, J. Teixeira, R. Sun, H.-L. Pan, J. K. Fletcher, and C. S. Bretherton, 2016: Implementation in the NCEP GFS of a hybrid eddy-diffusivity mass-flux (EDMF) boundary layer parameterization with dissipative heating and modified stable boundary layer mixing. *Wea. Forecasting*, **31**, 341–352, <https://doi.org/10.1175/WAF-D-15-0053.1>.
- Hong, S. Y., and H. L. Pan, 1996: Nonlocal boundary layer vertical diffusion in a medium-range forecast model. *Mon. Wea. Rev.*, **124**, 2322–2339, [https://doi.org/10.1175/1520-0493\(1996\)124<2322:NBLVDI>2.0.CO;2](https://doi.org/10.1175/1520-0493(1996)124<2322:NBLVDI>2.0.CO;2).
- Iacono, M. J., J. S. Delamere, E. J. Mlawer, M. W. Shephard, S. A. Clough, and W. D. Collins, 2008: Radiative forcing by long-lived greenhouse gases: Calculations with the AER radiative transfer models. *J. Geophys. Res.*, **113**, D13103, <https://doi.org/10.1029/2008JD009944>.
- Keper, J. D., 2012: Choosing a boundary layer parameterization for tropical cyclone modeling. *Mon. Wea. Rev.*, **140**, 1427–1445, <https://doi.org/10.1175/MWR-D-11-00217.1>.
- Li, X. L., and Z. X. Pu, 2008: Sensitivity of numerical simulation of early rapid intensification of Hurricane Emily (2005) to cloud microphysical and planetary boundary layer parameterizations. *Mon. Wea. Rev.*, **136**, 4819–4838, <https://doi.org/10.1175/2008MWR2366.1>.
- Nolan, D. S., D. P. Stern, and J. A. Zhang, 2009: Evaluation of planetary boundary layer parameterizations in tropical cyclones by comparison of in situ observations and high-resolution simulations of Hurricane Isabel (2003). Part II: Inner-core boundary layer and eyewall structure. *Mon. Wea. Rev.*, **137**, 3675–3698, <https://doi.org/10.1175/2009MWR2786.1>.
- Smith, R. K., and M. T. Montgomery, 2010: Hurricane boundary-layer theory. *Quart. J. Roy. Meteor. Soc.*, **136**, 1665–1670, <https://doi.org/10.1002/qj.679>.
- , and G. L. Thomsen, 2010: Dependence of tropical-cyclone intensification on the boundary-layer representation in a numerical model. *Quart. J. Roy. Meteor. Soc.*, **136**, 1671–1685, <https://doi.org/10.1002/qj.687>.
- Tallapragada, V., and Coauthors, 2015: Hurricane Weather Research and Forecasting (HWRf) Model: 2015 scientific documentation. Developmental Testbed Center Rep., 113 pp., [http://www.dtcenter.org/HurrWRF/users/docs/scientific\\_documents/HWRf\\_v3.7a\\_SD.pdf](http://www.dtcenter.org/HurrWRF/users/docs/scientific_documents/HWRf_v3.7a_SD.pdf).
- , and Coauthors, 2016: Forecasting tropical cyclones in the western North Pacific basin using the NCEP operational HWRf Model: Model upgrades and evaluation of real-time performance in 2013. *Wea. Forecasting*, **31**, 877–894, <https://doi.org/10.1175/WAF-D-14-00139.1>.
- Troen, I., and L. Mahrt, 1986: A simple-model of the atmospheric boundary layer; sensitivity to surface evaporation. *Bound.-Layer Meteor.*, **37**, 129–148, <https://doi.org/10.1007/BF00122760>.
- Vickers, D., and L. Mahrt, 2004: Evaluating formulations of stable boundary layer height. *J. Appl. Meteor.*, **43**, 1736–1749, <https://doi.org/10.1175/JAM2160.1>.
- Vickery, P. J., D. Wadhwa, M. D. Powell, and Y. Chen, 2009: A hurricane boundary layer and wind field model for use in engineering applications. *J. Appl. Meteor. Climatol.*, **48**, 381–405, <https://doi.org/10.1175/2008JAMC1841.1>.
- Wang, W., X. Shen, and W. Huang, 2016: A comparison of boundary-layer characteristics simulated using different parameterization schemes. *Bound.-Layer Meteor.*, **161**, 375–403, <https://doi.org/10.1007/s10546-016-0175-4>.
- Wang, Y. Q., 1995: An inverse balance equation in sigma coordinates for model initialization. *Mon. Wea. Rev.*, **123**, 482–488, [https://doi.org/10.1175/1520-0493\(1995\)123<0482:AIBEIS>2.0.CO;2](https://doi.org/10.1175/1520-0493(1995)123<0482:AIBEIS>2.0.CO;2).
- Zhang, J. A., and W. M. Drennan, 2012: An observational study of vertical eddy diffusivity in the hurricane boundary layer. *J. Atmos. Sci.*, **69**, 3223–3236, <https://doi.org/10.1175/JAS-D-11-0348.1>.
- , and E. W. Uhlhorn, 2012: Hurricane sea surface inflow angle and an observation-based parametric model. *Mon. Wea. Rev.*, **140**, 3587–3605, <https://doi.org/10.1175/MWR-D-11-00339.1>.
- , and F. D. Marks, 2015: Effects of horizontal diffusion on tropical cyclone intensity change and structure in idealized three-dimensional numerical simulations. *Mon. Wea. Rev.*, **143**, 3981–3995, <https://doi.org/10.1175/MWR-D-14-00341.1>.
- , —, M. T. Montgomery, and S. Lorsolo, 2011: An estimation of turbulent characteristics in the low-level region of intense Hurricanes Allen (1980) and Hugo (1989). *Mon. Wea. Rev.*, **139**, 1447–1462, <https://doi.org/10.1175/2010MWR3435.1>.
- , D. S. Nolan, R. F. Rogers, and V. Tallapragada, 2015: Evaluating the impact of improvements in the boundary layer parameterization on hurricane intensity and structure forecasts in HWRf. *Mon. Wea. Rev.*, **143**, 3136–3155, <https://doi.org/10.1175/MWR-D-14-00339.1>.